Lawrence Berkeley National Laboratory
LBL Publications

Title
Superresolution fluorescence mapping of single-nanoparticle catalysts reveals spatiotemporal variations in surface reactivity

Permalink
https://escholarship.org/uc/item/2np1n4m5

Journal
Proceedings of the National Academy of Sciences, 112(29)

ISSN
0027-8424

Authors
Zhang, Yuwei
Lucas, J. Matthew
Song, Ping
et al.

Publication Date
2015-07-06

eScholarship.org Powered by the California Digital Library
University of California

Superresolution fluorescence mapping of single-nanoparticle catalysts reveals spatiotemporal variations in surface reactivity

Yuwei Zhang[a,b,1], J. Matthew Lucas[c,d,1], Ping Song[a,b,1], Brandon Beberwyck[d,e], Qiang Fu[a,b], Weilin Xu[a,b,2], and A. Paul Alivisatos[d,f,g,2]

[a]State Key Laboratory of Electroanalytical Chemistry, Changchun Institute of Applied Chemistry, Chinese Academy of Science, Changchun 130022, People's Republic of China; [b]Jilin Province Key Laboratory of Low Carbon Chemical Power, Changchun Institute of Applied Chemistry, Chinese Academy of Science, Changchun 130022, People's Republic of China; [c]Department of Mechanical Engineering, University of California at Berkeley, CA 94720; [d]Materials Science Division, Lawrence Berkeley National Laboratory, Berkeley, CA 94720; [e]Department of Materials Science and Engineering, University of California at Berkeley, CA 94720; [f]Department of Chemistry, University of California at Berkeley, CA 94720; and [g]Kavli Energy Nano Science Institute, University of California, Berkeley, CA 94720

Edited by Alexis T. Bell, University of California, Berkeley, CA, and approved June 19, 2015 (received for review January 30, 2015)

For the practical application of nanocatalysts, it is desirable to understand the spatiotemporal fluctuations of nanocatalytic activity at the single-nanoparticle level. Here we use time-lapsed superresolution mapping of single-molecule catalysis events on individual nanoparticles to observe time-varying changes in the spatial distribution of catalysis events on Sb-doped TiO_2 nanorods and Au triangle nanoplates. Compared with the active sites on well-defined surface facets, the defects of the nanoparticle catalysts possess higher intrinsic reactivity but lower stability. Corners and ends are more reactive but also less stable than flat surfaces. Averaged over time, the most stable sites dominate the total apparent activity of single nanocatalysts. However, the active sites with higher intrinsic activity but lower stability show activity at earlier time points before deactivating. Unexpectedly, some active sites are found to recover their activity ("self-healing") after deactivation, which is probably due to desorption of the adsorbate. Our superresolution measurement of different types of active catalytic sites, over both space and time, leads to a more comprehensive understanding of reactivity patterns and may enable the design of new and more productive heterogeneous catalysts.

single-molecule nanocatalysis | optical superresolution imaging | photocatalysis | surface restructuring

All kinds of nanoparticles, such as metals, metal oxides, and even nonmetals, are used as catalysts in a variety of chemical processes (1). In support of developing better and less-expensive nanoparticle catalysts, single-molecule mapping of nanocatalyst activity using superresolution imaging at the single-nanoparticle level can determine active site locations on nanoparticles and which structures are most reactive (2–5). For example, defects, corners, and edges on nanoparticle surfaces have been shown by single-molecule, superresolution imaging of single nanocatalysts to be more active than other sites. The relative abundance of these sites on nanoparticle catalysts is important for explaining their observed reactivity (2, 4, 6–13).However, prior reports are based on long-time integrations of catalytic activity and thus do not provide information about any dynamic changes in catalytic activity, such as the time-dependent evolution of different active sites. Studies of time-varying catalytic activity are thus arguably more informative than time-averaged observations.

The temporal fluctuation of catalytic activity on nanocatalysts or electrodes has been previously observed in situ at both the ensemble and single-nanoparticle level (14–17). More recently, superresolution imaging techniques have been applied to identify the spatial distribution of catalytic activity on a few different nanocatalysts including $Au@SiO_2$ nanorods, $Au@SiO_2$ nanotriangles (2, 4) and Au–CdS nanohybrids (6). The observed spatial variations in catalytic activity between different catalysts were merely attributed to possible reaction-driven surface reconstruction of the nanocatalysts, possibly owing to the different types of surface atoms (14, 15). Is there a more specific explanation for the fluctuations or the static spatial distributions in reactivity of nanocatalysts?

In this work we show time-lapsed, superresolution mapping with single-product-molecule sensitivity, which can elucidate spatial changes in catalytic activity over time. Our time-lapsed study, despite its coarse temporal resolution, allows deeper understanding of catalytic activity by observing fluctuations in catalytic activity among active sites on a single nanocatalyst.

Results and Discussion

Our superresolution imaging of catalytic reactions is based on wide-field single-molecule fluorescence microscopy of two fluorogenic catalytic reactions (2, 4, 18). For the first experiment, we chose high aspect ratio, Sb-doped TiO_2 nanorods (diameter, ~3 nm; length, 90~150 nm, Fig. 1*A*) as the photocatalysts. These were synthesized according to literature with minor modification (19) (*SI Appendix*, Figs. S1 and S2). Sb-doped TiO_2nanorods can be excited with green (514-nm) light (18) to generate electron (e^-)/hole (h^+) pairs (*SI Appendix*, Fig. S3). The photogenerated electrons and holes produce adsorbed hydroxyl radicals ($OH^{\bullet}_{ads}$) and superoxide anion radicals ($O^{-\bullet}_{2ads}$) on nanorod surface, respectively, by further reaction with H_2O_{ads}/OH^-_{ads} or O_{2ads}. These adsorbed radicals subsequently oxidize Amplex Red into its fluorescent product, resorufin (Fig. 1*B*) by breaking the *N*–C bond in the substrate molecule. The dynamics of this reaction

Significance

Here we use time-lapsed superresolution mapping of single-molecule catalysis events on individual nanoparticle surface to observe time-varying changes in the spatial distribution of catalysis events on Sb-doped TiO_2 nanorods and Au triangle nanoplates. The ability to measure both the spatial- and time-resolved activity of different types of active sites on single-nanoparticle surface leads to a more comprehensive understanding of reactivity patterns and may enable the design of new and more productive heterogeneous catalysts.

Author contributions: W.X. and A.P.A. designed research; Y.Z. and P.S. performed research; J.M.L., P.S., B.B., Q.F., and W.X. contributed new reagents/analytic tools; Y.Z., J.M.L., P.S., B.B., and W.X. analyzed data; and Y.Z., J.M.L., W.X., and A.P.A. wrote the paper.

The authors declare no conflict of interest.

This article is a PNAS Direct Submission.

[1]Y.Z., J.M.L., and P.S. contributed equally to this work.

[2]To whom correspondence may be addressed. Email: weilinxu@ciac.ac.cn or alivis@berkeley.edu.

This article contains supporting information online at www.pnas.org/lookup/suppl/doi:10.1073/pnas.1502005112/-/DCSupplemental.

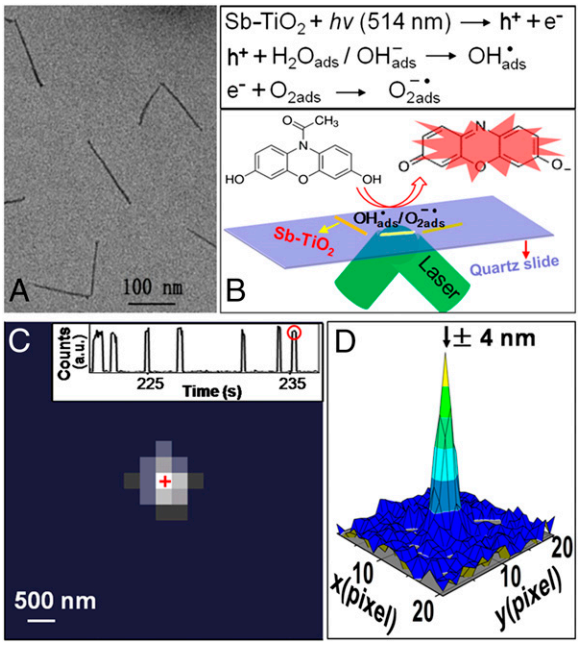

Fig. 1. Single-molecule superresolution fluorescence microscopy of Sb-doped TiO_2 nanorod photocatalyst at single-turnover resolution. (*A*)Typical TEM image of Sb-doped TiO_2 nanorods. (*B*, *Top*) Formation of reactive radicals from the photogenerated electrons and holes. (*Bottom*) TIRF microscopy to image the fluorogenic reaction of Amplex Red to resorufin photocatalyzed by individual Sb-doped TiO_2 nanorods. (*C*) Wide-field fluorescence image of a single resorufin molecule during one burst. (*Inset*) The red circle indicates part of a typical fluorescence intensity versus time trajectory for a single Sb-doped TiO_2 nanorod with 1-μM Amplex Red in the reactant solution. (*D*) Three-dimensional representation of the image in *C*. The fluorescence intensity of a single-product molecule spreads over a few pixels (each pixel, ~267 nm) as a point-spread function (PSF). The center position of this PSF can be localized with nanometer accuracy and is marked as a red cross in *C*.

system have been previously studied at the single-molecule single-nanoparticle level (18).

Here we use a superresolution imaging approach to study the location of the individual resorufin molecules formed on a single nanocatalyst. To image this reaction on single Sb-doped TiO_2 nanorods, we sparsely disperse the nanorods on a quartz slide in a microflow cell and supplied the reactants in a constant flow (Fig. 1*B* and *SI Appendix*). Under a total internal reflection fluorescence (TIRF) microscope, each catalytic reaction generates a fluorescent resorufin molecule, whose laser (514-nm)-induced fluorescence on top of the nanorods is imaged on an electron-multiplying charge-coupled device camera with an integration time of 100 ms.

Fig. 1*C* (*Inset*) shows part of a typical fluorescence intensity vs. time trajectory from a single Sb-doped TiO_2 nanorod. Each burst corresponds to one product molecule (i.e., one catalytic turnover) and the duration of each burst corresponds to the time each resorufin molecule spends on the nanocatalyst before it desorbs, diffuses away from the active site, and leaves the TIRF excitation field. Fig. 1*C* shows the fluorescence image of a single resorufin molecule in one burst indicated by a red circle (*Inset*). Owing to diffraction, the fluorescence signal of a single molecule spreads over a few camera pixels (each pixel ~267 nm), even though the resorufin molecule is only about 1 nm in size. However, if a sufficient number of fluorescence photons are collected, we can localize the center position of the fluorescent molecule to nanometer accuracy by fitting its fluorescence image with a point-spread function based on a 2D Gaussian function (Fig.1*D* and *SI Appendix*) (2, 4). By localizing the positions of individual fluorescent resorufin molecules from these bursts of fluorescence, we are able to map where the resorufin molecules formed and thus locate the active sites on a single nanocatalyst. Because we have a time series of such catalytic activity maps, we can visualize the fluctuations in reactivity on a single nanocatalyst over time.

By localizing the position of each product molecule generated over a long period (up to 13 h in 20+ sequential movies), we mapped about 10,000 catalytic events on a single Sb-doped TiO_2 nanorod (Fig. 2). Both this map and the 2D histogram (Fig. 2*N*) of product positions resolve the rod shape with ~20-nm resolution (*SI Appendix*, Figs. S4 and S5). This is comparable resolution to related superresolution optical microscopy techniques (2, 11). Furthermore, the wide-field imaging format of our approach offers the capability to study multiple nanorods in the same frame, thus providing higher data collection efficiency. Similar imaging techniques have also been used in long-time–averaged analyses to differentiate catalysis on different facets of metal hydroxide and oxide microcrystals (6, 9, 12), resolve catalytic domains (13), and map static spatial patterns of reactivity (2, 4).

The location where catalytic events occur changes systematically over the observation time period (Fig. 2). Initially, products are formed near the center of the nanorod (Fig. 2*A*), then the ends become preferential (Fig. 2 *B*–*E*). Fig. 2 *J* and *N* shows a distribution of product molecules over a larger spatial area than the real dimension of the nanorod, which is only ~125 nm long and 3 nm in diameter (*SI Appendix*, Fig. S2). The reason for this apparent spreading of products could be attributed to both the random slow diffusion of dye molecules in the boundary layer around the nanoparticle surface on the timescale of a few hundreds of milliseconds (one burst) after their formation on the active sites (*SI Appendix*, Fig. S6) and the limited resolution (~20 nm) of our imaging technique (6) (*SI Appendix*, Fig. S5). Whereas we expect that surface-adsorbed products will have reduced diffusion (20–22), free resorufin in a boundary layer (*SI Appendix*) is calculated to diffuse tens of nanometers from the active sites on the timescale of 100 ms, as shown schematically in Fig. 2*O*. Interestingly, the 1D histogram distribution in the y direction (Fig. 2*J*) along the long axis of the nanorod clearly shows two peaks. If we take the two peaks of the histogram to be the ends of the nanorod, we can approximately determine the location of the nanorod as indicated by the red bar. Fig. 2*N* shows these two ends produce more product molecules than the middle of this nanorod. The top end also produces more products than the bottom end. Over long times, the two ends of the nanorod are more productive than the middle, although the two ends are not equally active. This heterogeneous distribution of reactivity or active sites on single nanocatalysts has been extensively observed in other single-nanocatalyst systems (2, 4, 9, 11) and is in agreement with a recent report on 1D SiO_2-coated Au nanorods (2).

To observe the evolution of spatial patterns of reactivity on this nanorod, the total number of product molecules detected was divided into 5 portions, each containing about 2,000 molecules, each representing a single catalytic event; 2,000 events is about 3 h. The locations of these single catalytic events are plotted in 2D histograms with a different color for each of the five portions (denoted p1 through p5) as shown in Fig. 2 *A*–*E*. Strikingly, the image sequence shows the first portion of product molecules is mainly formed on the middle part of the nanorod with a corresponding turnover rate of 0.22 ± 0.01 s^{-1} (Fig. 2*A* and *SI Appendix*, Fig. S7), whereas the second portion of product molecules (Fig. 2*B*) is mainly formed on the two ends of the nanorod [turnover frequency (TOF) =0.20 ± 0.01 s^{-1}]. The top end of the nanorod is more active than the bottom end, which indicates a fluctuation in spatial reactivity over time on this single nanorod. During p2, the reactivity of the middle of the nanorod decreased compared with p1. This is probably due to

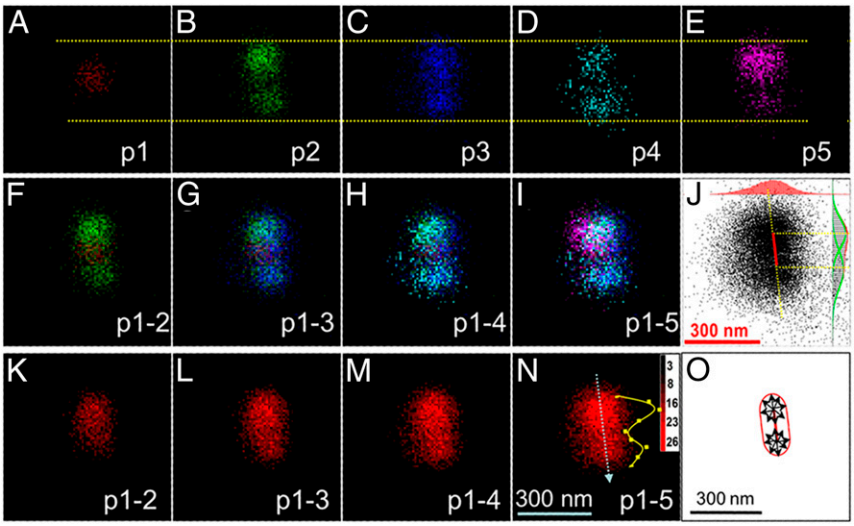

Fig. 2. Time-sequence single-molecule catalysis mapping on a single Sb-doped TiO_2 nanorod in 10×10 nm^2 bins. (*A–E*) The time sequence of 2D histograms of every 2,000 product molecules. Different colors indicate different portions of product molecules obtained in the time sequence [(*A*) p1: the first 2,000 product molecules; (*B*) p2: the second 2,000 product molecules; (*C*) p3: the third 2,000 product molecules; (*D*) p4: the fourth 2,000 product molecules; and (*E*) p5: the fifth 2,000 product molecules]. (*F–I*) The overlapping of different portions. (*F*) (p1-2) or (p1+p2); (*G*) (p1-3) or (p1+p2+p3); (*H*) (p1-4); (*I*) (p1-5). (*J*) Positions of product molecules detected on the nanorod in *I*. (*Insets*) Histogram distribution in both X (up) and Y (right) directions. (*K–N*) The 2D histograms of different numbers of product molecules obtained on the rod at different time: (*K*) The first 4,000 product molecules; (*L*) The first 6,000 product molecules; (*M*) The first 8,000 product molecules; (*N*) All of the (around 10,000) product molecules; (*Inset*) Intensity distribution along the long-axis direction. (*O*) Scheme to show the limited spatial-resolution and molecule diffusion-induced smearing of the outline of the nanorod.

the fast deactivation of the active sites with higher initial activity. On the other hand, the two ends could become dominant gradually after an incubation period (1).

As time progresses to p3 (Fig. 2*C*), product molecules were formed almost evenly on the two ends (TOF = 0.18 ± 0.01 s^{-1}). During p4 (Fig. 2*D*), the bottom end became slightly more active than the top end (TOF = 0.17 ± 0.01 s^{-1}). During p5 (Fig. 2*E*), the top end becomes more active (TOF = 0.17 ± 0.01 s^{-1}), which is the reverse of the activity during p4. The above trends can be seen more vividly when we overlay these color images one by one in time sequence, as shown in Fig. 2 *F–I*. Similar results can be seen when a single 2D histogram plot contains more and more product molecules, as shown in Fig. 2 *K–N*.

From Fig. 2 *A–E*, the following observations are clear: (*i*) At the beginning of reaction, the middle part of the nanorod possesses higher initial reactivity for photocatalysis than the two ends. (*ii*) Compared with the two ends, the middle part of the rod shows photoreactivity first. It also deactivates first. (*iii*) There is an incubation time before the ends become dominant, and once dominant, their relative reactivities fluctuate with time. One end can be more active than the other end but then switch. (*iv*) Considering time-averaged observations, the two ends of the nanorod dominate the overall reactivity because they have better stability than the middle of the rod, despite their lower apparent reactivity compared with the middle of the rod. This suggests that over long-time observations, the products formed on nanocatalysts are mainly due to stable, modestly active sites rather than unstable, active sites with higher reactivity.

Similar fluctuations of the four observations stated above in the spatial location of high activity have been observed across multiple ($n = 83$) individual Sb-doped TiO_2 nanorods analyzed as in Fig. 2. For example, the middles of these individual nanorods show comparable or higher initial productivity than the ends (*SI Appendix*, Fig. S8). Interestingly, besides the similarity, these additional observations show slightly different patterns of fluctuating activity. For instance, *SI Appendix*, Fig. S9 shows another nanorod with much longer incubation time before the ends become dominant compared with the nanorod shown in Fig. 2. More interestingly, *SI Appendix*, Fig. S9*E* shows that the reactivity of the middle part of this nanorod can recover spontaneously after several hours in a deactivated state. Similar behavior has been observed more frequently at the nanorod ends (Fig. 2).This recovery of catalytic activity, which we term "self-healing," suggests that deactivation of active sites on the nanorod is reversible, which is probably due to the desorption of an adsorbate. Alternatively, the above fluctuations were also observed from the time-dependent aspect ratio of the distribution of localization events on individual nanorods(*SI Appendix*, Figs. S10–S14). Our repeated observations of spatiotemporal changes in activity across individual nanorods suggest such fluctuations are a general phenomenon for this type of Sb-doped TiO_2 nanocatalyst. Such time-dependent observations on single nanocatalysts have never, to our knowledge, been observed before because all prior studies analyzed time-averaged data (2, 4, 6, 11), similar to the long-time–averaged images in Fig. 2 *N* and *J*.

The oscillating catalytic activity of particular areas of the nanorod has at least two possible explanations. First, the large number of ~2-eV laser excitations incident upon the rod do not all result in catalytic activity. Whereas these photons have very little energy compared with the volume of the rod, the excitation may be sufficient to occasionally create low coordination sites on the ends (more probable), or even, less probably, in the center. These new low coordination sites may be transient, although highly active, catalytic sites. Therefore, one strategy for increasing overall catalytic activity may be to seek systems more easily perturbed by illumination due to their lower cohesive energy per atom. Second, dynamics of surface adsorbates may explain the recovery in catalytic activity. For example, when Amplex Red is oxidized to resorufin, a chemical group (-C(O)-CH_3) is released, which may adsorb on the surface. This adsorbate could block an otherwise active catalytic site. Its binding may lead to surface reorganization too. Similar adsorbate-induced surface reorganization is observed in other systems such as CO on a Pt(557) single crystal (23) and PtSn nanoparticles (24). Either of these hypotheses may explain the observed self-healing of the nanorods.

The spatiotemporal single-molecule mapping of catalytic activity reveals the dynamic fluctuation of reactivity patterns on single nanocatalysts. These fluctuations are significant for trying to rationally develop higher-efficiency functional materials. To understand the origin of the fluctuating reactivity across a single Sb-doped TiO_2 nanorod, we characterized the morphology of TiO_2 nanorods with transmission electron microscopy (TEM) in an effort to identify structural heterogeneity across the nanorod that may explain the different catalytic activities observed.

Several dozen nanorods were imaged and were all found to be monocrystalline according to fast Fourier transforms taken along their lengths. Although monocrystalline, the nanorods display variations in thickness, sidewall uniformity, and end shapes including flat, tapered, and bulbous morphologies (*SI Appendix*, Fig. S15). Variability of catalytic activity across a substrate has been strongly correlated to structural inhomogeneities (25); therefore, the tiny structural heterogeneity of nanorods may be partially responsible for the heterogeneous catalytic activity observed across individual nanorods. Although no nanorod end exhibits a different crystallographic orientation, some diffract weakly or not at all (*SI Appendix*, Fig. S16). That may be an imaging artifact, but may also be an indication the rod ends are amorphous. These unusual structures may be uniquely active, or they may merely increase the number of undercoordinated sites near the rod end. Taken together, these variations and their accompanying surface atom coordination may explain the enhanced catalytic activity at the rod ends.

The early and intrinsically high activity of the middle part of the nanorod may also be explained by structural factors. For instance, some of the rods have very smooth sides whereas others have rough sides. Some of the rods are visibly tapered whereas others have a more uniform diameter (*SI Appendix*, Figs. S15 and S16). Seed-mediated growth may have a role in this atomic-scale irregularity in the middle of the rod because the longer nanorods were grown from shorter nanorods (*SI Appendix*, Figs. S1 and S2). In a seed-mediated growth, the middle section of the resulting nanorod grows faster than the two ends (26). The faster growth rate may lead to a higher density of defects in the middle of the nanorod (2, 27). The higher density or the larger number of defects could account for the transient high productivity or activity of that area (Fig. 2*A*) because the crystallographic defects could serve as active sites (1, 4, 28). Unfortunately, the short catalytic lifetime of the middle section indicates these active sites, whatever their origin, are relatively unstable. It is well known that sites with high activity are usually less stable and easier to deactivate than sites with comparatively lower reactivity (1, 14). The difference in catalytic lifetime between the middle section and ends of the nanorod explains prior static observations of low reactivity in the middle section of the single nanorod. Static observations of greater time-averaged reactivity at the nanorod ends can be explained by the relative abundance of low-coordination sites, such as corners and edges, which are often more reactive because of their large coordinative unsaturation (1). The ends of TiO_2 nanorods generally have a higher percentage of corner and edge sites and consequently higher time-averaged catalytic reactivity (2).

The incubation time observed on the nanorod ends (Fig. 2*B*) has at least two possible explanations. First, there could initially be few active sites on the two ends, but as the reaction proceeds on the middle part it induces spontaneous, reaction-driven surface reconstruction (14) that leads to the formation of new active sites on ends. The newly formed active sites subsequently show activity. The second explanation is that the active sites on the rod ends are initially deactivated by some inert adsorbates which gradually desorb over time and allow those end sites to become collectively more active. Both of these explanations allow for the deactivation of the middle of the rod and emergent activity of the rod ends.

To further confirm that dynamic fluctuations of reactivity patterns on single nanocatalysts are not limited to Sb-doped TiO_2 nanorods, we applied the same superresolution single-molecule imaging technique to single Au triangle nanoplates. Au nanoparticles are known to effectively catalyze the reduction of resazurin by NH_2OH to form a fluorescent product, resorufin (Fig. 3*A*) (14). The flat single-crystalline gold nanoplates with stacking faults (29, 30) (*SI Appendix*, Figs. S17–S20) were synthesized according to literature (31) with side length of 160 ± 20 nm (*SI Appendix*, Fig. S21), thickness of about 8 nm (*SI Appendix*, Fig. S22), and are transparent to light (2, 4).

Single-molecule superresolution imaging over long periods (up to 10 h) mapped the reactivity pattern of individual Au nanoplates (Fig. 3*B*). Interestingly, the time-integrated image shows the outline of a triangle, consistent with the Au nanoplates shown in *SI Appendix*, Fig. S17*A*. The center area shown in Fig. 3*B* is brighter than corners or edges, which indicates greater integrated catalytic activity in the center area of the Au nanoplate than on the edges.

To quantitatively show the static differences in activity across this Au nanoplate, the activity from the particle's center to each corner is plotted in Fig. 3*B* (*Inset*), which shows an approximately linear activity gradient from the center to the three corners of the nanoplate. Due to the seed-mediated growth of the Au nanoplates (31) and consistent with a prior report (2), we deduce that the center area of the nanoplate around the seed grows faster than the peripheral corners and edges (26, 27). The faster growth rate near the center may lead to a higher density of defects, which are often the active sites for heterogeneous catalysis (1). There may also be a stacking fault parallel to the (*111*) facet (*SI Appendix*, Fig. S17) that contributes to terraces and other features on the otherwise flat (*111*) facet that would enhance its catalytic activity.

To explore the spatiotemporal variations in activity across a single Au nanoplate, we completed sequential mapping of individual catalytic events in the same manner as the single TiO_2 nanorod (Fig. 2 *A–E*). All of the catalytic product locations shown in Fig. 3*B* were split into five subgroups containing the same number of observed product molecules, denoted as p1, p2, p3, p4, and p5, respectively. Each portion was then plotted in a 2D histogram distribution with a different color as shown in Fig. 3 *C–G*. Fig. 3 *H–K* corresponds to the one-by-one overlapping from (*H*) p1 to p2; (*I*) p1 to p3; (*J*) p1 to p4, and (*K*) p1 to p5, respectively. Fig. 3 *M–Q* shows the 2D plots with increasing numbers of product molecules. Interestingly, the outline of the Au triangle nanoplate becomes more apparent as additional product molecules are added to the 2D histogram (Fig. 3 *K* and *Q*, triangular nanoplate outlined to aid the reader). The image sequence from Fig. 3*C–G* shows that product molecules are initially formed at the top corner (TOF = 0.17 ± 0.01 s^{-1}) (Fig. 3*C*), indicating the active domain is initially located on this corner of the Au nanoplate. At later time (Fig. 3*D*) the whole surface becomes active (TOF = 0.15 ± 0.01 s^{-1}) with the center area becoming dominant. Later (Fig. 3*E*), the top corner almost completely deactivates and the reactive domain drifts to the bottom of the nanoplate (TOF = 0.15 ± 0.01 s^{-1}), close to one edge. In the last two portions, the active area remains roughly centered while drifting slightly toward the right corner (TOF = 0.14 ± 0.01 s^{-1}) (Fig. 3 *F* and *G*). Control experiments show turnover frequency is not affected by laser intensity. Furthermore, reductant in the flow cell is found to be necessary for formation of luminescent resorufin. We therefore conclude that electron transfer from the Au nanoparticle is not the source of the reducing species in the flow cell.

From the time-averaged 2D histogram (Fig. 3*B*), we can see that the center area of the nanoplate shows higher activity compared with the corners or edges. These observations indicate the following: (*i*) The three corners are not equally active

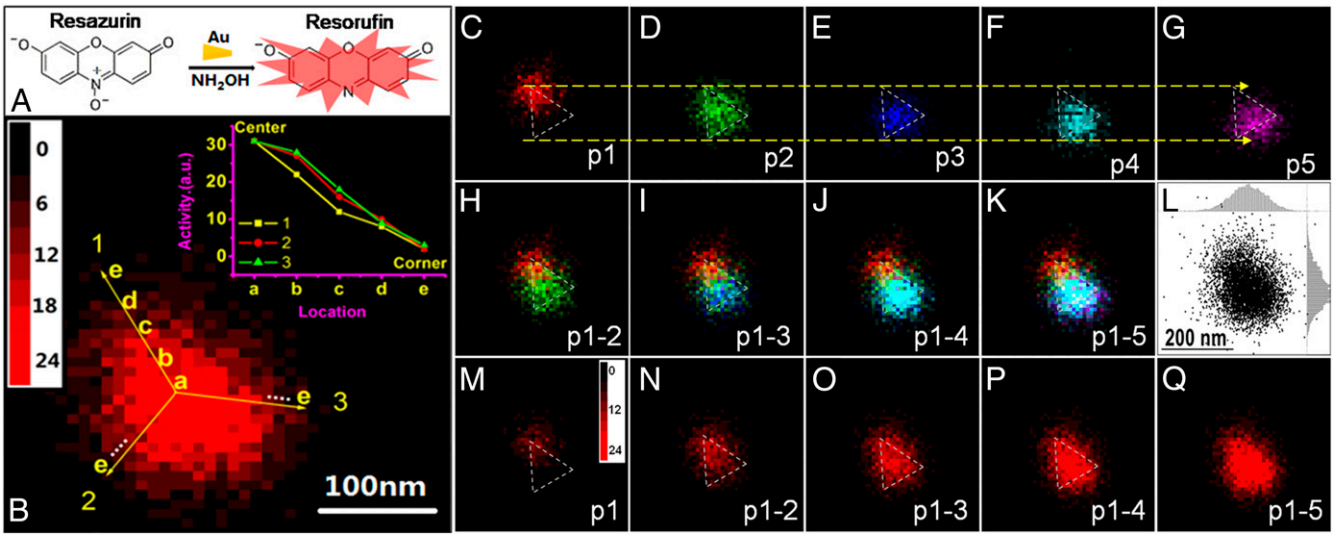

Fig. 3. Time-lapsed single-molecule catalysis mapping on single Au nanoplate in 10 × 10 nm^2 bins. (*A*) Fluorogenic reaction of resazurin reduced to resorufin by NH_2OH catalyzed by Au nanoplates. (*B*) The 2D histogram of product molecules obtained on a Au nanoplate. (*Inset*) Gradient descent of activity along the three corners from the center of the Au nanoplate. (*C*–*G*) Sequential 2D histograms of every 1,000 product molecules. Different colors indicate different portions of product molecules obtained in time sequence: (*C*) p1: the first 1,000 product molecules; (*D*) p2: the second 1,000 product molecules; (*E*) p3: the third 1,000 product molecules; (*F*) p4: the fourth 1,000 product molecules; and (*G*) p5: the fifth 1,000 product molecules. (*H*–*K*) The overlapping of different portions: (*H*) (p1-2); (*I*) (p1-3); (*J*) (p1-4); (*K*) (p1-5). (*L*) Positions of product molecules detected on the nanoplate in *K*. (*Insets*) Histogram distribution in both X (up) and Y (right) directions. (*M*–*Q*) The 2D histograms with different numbers of product molecules obtained on the rod at different time: (*M*) the first 1,000 product molecules; (*N*) the first 2,000 product molecules; (*O*) the first 3,000 product molecules; (*P*) the first 4,000 product molecules; (*Q*) All of the observed (around 5,000) product molecules.

initially. This could be attributed to the heterogeneous imperfections of these corners (31, 32). However, over time all three corners show similar reactivity (Fig. 3*B*). (*ii*) Some corners show activity earlier than others, which indicates these corners possess higher initial transient activity than other areas on the nanoplate. (*iii*) The highly reactive corners show activity first, but also deactivate sooner, indicating the active sites with higher reactivity are usually less stable compared with the active sites with lower reactivity. This is similar to the pattern observed on Sb-doped TiO_2 photocatalysts shown in Fig. 2. (*iv*) Over long observation periods, the reactivity of the center of the nanoplate is more productive than the edges and corners. The higher activity of the center (*111*) facet may be attributable to defects due to the seed-mediated growth of the Au nanoplates or may be related to a likely stacking fault across the flat facet of the nanoplate. Interestingly, all four of these observations are qualitatively present on multiple (n = 67) individual Au nanoplates. Another nanoplate is shown in *SI Appendix*, Fig. S23. The time-dependent aspect ratio of the distribution of localization events on individual nanoplates was also studied but not much information could be obtained (*SI Appendix*, Figs. S24–S26).

To further understand the spatiotemporal fluctuation of activity of single Au nanoplates observed above, ex situ TEM was performed to study the catalysis-induced surface reconstruction on single Au nanoplates. As shown in *SI Appendix*, Fig. S27, after a long catalytic process (~8 h; *SI Appendix*) some corners or edges on nanoplates are altered. The corners (marked with *, #, and @) varied from sharp to blunt and the edges (marked with arrows and circles) varied from straight to chamfered. The extent of variation among these three sites is consistent with the catalytic reactivity order: corner > edge > center, which is consistent with catalysis-induced reconstruction. Furthermore, *SI Appendix*, Fig. S27 also shows, after the long catalytic process, that some nanoplates show observable blunting on all of the three corners just like those indicated by red circles and symbol @, whereas some others only show obvious blunting on one (noted with *) or two corners (noted with #). These observations of substantial shape change near the corners and edges of the same nanoplates serve as empirical evidence for structural transformations that would explain the behavior observed in Fig. 3 *C*–*Q*. Such changes in shape cannot exclude the possibility that gradual adsorption or desorption of inert adsorbates on active sites plays a role in their deactivation, but the obvious structural transformations present in the nanoplates after catalysis suggest adsorbates have a minor effect.

Our static observations of reactivity patterns on Au nanoplates are consistent with previous observations that surface defects play an important role in catalytic activity on individual SiO_2-coated Au nanorods (2). In that study, Zhou et al. found a gradient of catalytic activity consistent with a distribution of defects along the sides of Au nanorods. However, on large (>500 nm) SiO_2-coated Au nanoplates (4), the same group observed the opposite activity gradient (i.e., activity of corner > edge > center) that we observed on the Au nanoplates (activity of center > edge or corners). The difference is likely explained by the differences in samples—our observation was on naked Au triangle nanoplates whereas the prior reports were on SiO_2-coated Au nanoplates (4). In that work, the nanoplates were covered with a porous layer of SiO_2 about 45 nm thick with a random distribution of nanopores (2). Based on insights from molecular dynamics simulations (33), differences in strain or other imperfections across the porous SiO_2 nanolayer create more cracks at the corners and edges than on the center section of the nanoplate that is flat and smooth. As a result, the protective SiO_2 shell better shields the flat center area than the corners and edges. This less-cracked shell over the flat center area makes most of the Au reactive sites inaccessible to reactants. In this way, the apparent activity of the flat area is lower than the corners (4). In contrast, the naked Au nanoplates used in this work have two flat sides completely exposed to reactants so the larger number of active sites, possibly due to seed-mediated defects, makes the center area appear dominant over the edges and corners. In this case, the intrinsic activity per active site on the corners and edges is probably higher that on the flat sides but the larger number of active sites with higher stability on sides dominates the total reactivity of single nanoplates over a time.

We have observed, for the first time, to our knowledge, the in situ dynamic spatiotemporal fluctuations of reactivity patterns on single nanocatalysts. Without temporal resolution, one only can see the static (time-averaged) reactivity pattern of single nanocatalysts (2, 4, 34, 35). Clearly the dynamic fluctuations contain more information than a static averaged result. Previously, the dynamic reactivity fluctuation observed on single nanoparticles or at ensemble level was merely attributed to catalysis- or reaction-driven surface reconstruction, a process that occurs on a timescale of tens of seconds (14, 15). Our results reveal that besides surface reconstruction, the dynamic fluctuation of reactivity patterns also varies on a timescale of hours, mainly due to different natural catalytic properties of different types of reactive sites on single nanocatalysts. This additional source of variability is an important reason for the dynamic fluctuations of reactivity on single nanocatalysts and must be considered along with fast surface reconstruction when evaluating the overall reactivity of a nanocatalyst, as shown in *SI Appendix*, Fig. S28.

Conclusions

In summary, based on time-lapsed, single-molecule, superresolution mapping of individual nanocatalyst particles, we observed the dynamic spatiotemporal activity patterns on single nanocatalysts. In Sb-doped TiO_2 nanorods, we find that the middle parts of the nanorods possess higher transient productivity than the ends, which is likely due to the higher density or the larger number of defect sites, although these defect sites are unstable compared with those on the ends. In Au nanoplates, the corners are more reactive but also less stable than defects near the center of particles. The loss of activity near the corners is likely attributable to structural reorganization that blunts those sharp features. Integrated over long observation times, the more stable active sites dominate the total productivity of the nanocatalyst. The active sites with higher intrinsic activity but less stability show only short-lifetime activity at the early stages of the catalytic reaction. In the case of the nanorods, their activity can regenerate spontaneously after some time in an inactive state. The different properties of these different types of active sites lead to fluctuating patterns of reactivity the same way catalysis-induced surface reconstruction does. These previously unidentified observations imply one should pay more attention to the stable rather than more highly active but less stable sites when evaluating or developing new catalysts.

Methods

TiO_2 nanorods were synthesized with oleic acid and titanium isopropoxide and then doped with Sb based on Tris (dimethylamido) antimony. Au nanoplates were synthesized based on a seeded growth with reagents sodium citrate, $HAuCl_4$ and $NaBH_4$. Single-molecule superresolution imaging was based on a TIRF fluorescence microscopy (*SI Appendix*).

ACKNOWLEDGMENTS. Work was funded by the National Basic Research Program of China (973 Program, 2012CB932800 and 2014CB932700), National Natural Science Foundation of China (21273220, 21303180, and 201422307), and "The Recruitment Program of Global Youth Experts" of China. J.M.L. is supported as part of the Light-Material Interactions in Energy Conversion, an Energy Frontier Research Center funded by the US Department of Energy (DOE) Office of Science under Contract DE-SC0001293. B.B. was supported by a Fellowship from the DOE Office of Science Graduate Fellowship Program (DOE SCGF) under Contract DEAC05-06OR23100.

1. Somorjai GA, Li Y (2010) *Introduction to Surface Chemistry and Catalysis* (Wiley-Interscience, New York).
2. Zhou X, et al. (2012) Quantitative super-resolution imaging uncovers reactivity patterns on single nanocatalysts. *Nat Nanotechnol* 7(4):237–241.
3. Weckhuysen BM (2009) Chemical imaging of spatial heterogeneities in catalytic solids at different length and time scales. *Angew Chem Int Ed Engl* 48(27):4910–4943.
4. Andoy NM, et al. (2013) Single-molecule catalysis mapping quantifies site-specific activity and uncovers radial activity gradient on single 2D nanocrystals. *J Am Chem Soc* 135(5):1845–1852.
5. Rust MJ, Bates M, Zhuang X (2006) Sub-diffraction-limit imaging by stochastic optical reconstruction microscopy (STORM). *Nat Methods* 3(10):793–795.
6. Ha JW, et al. (2014) Super-resolution mapping of photogenerated electron and hole separation in single metal-semiconductor nanocatalysts. *J Am Chem Soc* 136(4): 1398–1408.
7. Naito K, Tachikawa T, Fujishima A, Majima T (2008) Real-time single-molecule imaging of spatial and temporal distribution of reactive pxygen species with fluorescent probes: Applications to TiO_2 photocatalysts. *J Phys Chem C* 112(4):1048–1059.
8. Tachikawa T, Majima T (2009) Exploring the spatial distribution and transport behavior of charge carriers in a single titania nanowire. *J Am Chem Soc* 131(24): 8485–8495.
9. Tachikawa T, Yamashita S, Majima T (2011) Evidence for crystal-face-dependent TiO_2 photocatalysis from single-molecule imaging and kinetic analysis. *J Am Chem Soc* 133(18):7197–7204.
10. Wang N, Tachikawa T, Majima T (2011) Single-molecule, single-particle observation of size-dependent photocatalytic activity in Au/TiO_2 nanocomposites. *Chem Sci (Camb)* 2(5):891–900.
11. Tachikawa T, Yonezawa T, Majima T (2013) Super-resolution mapping of reactive sites on titania-based nanoparticles with water-soluble fluorogenic probes. *ACS Nano* 7(1): 263–275.
12. Roeffaers MB, et al. (2006) Spatially resolved observation of crystal-face-dependent catalysis by single turnover counting. *Nature* 439(7076):572–575.
13. Roeffaers MBJ, et al. (2009) Super-resolution reactivity mapping of nanostructured catalyst particles. *Angew Chem Int Ed Engl* 48(49):9285–9289.
14. Xu W, Kong JS, Yeh Y-TE, Chen P (2008) Single-molecule nanocatalysis reveals heterogeneous reaction pathways and catalytic dynamics. *Nat Mater* 7(12):992–996.
15. Tao F, et al. (2008) Reaction-driven restructuring of Rh-Pd and Pt-Pd core-shell nanoparticles. *Science* 322(5903):932–934.
16. Imbihl R, Ertl G (1995) Oscillatory kinetics in heterogeneous catalysis. *Chem Rev* 95(3): 697–733.
17. Krischer K, Eiswirth E, Ertl G (1992) Oscillator CO oxidation on Pt(110): Modeling of temporal self-organization. *J Chem Phys* 96(12):9161–9172.
18. Xu W, Jain PK, Beberwyck BJ, Alivisatos AP (2012) Probing redox photocatalysis of trapped electrons and holes on single Sb-doped titania nanorod surfaces. *J Am Chem Soc* 134(9):3946–3949.
19. Joo J, et al. (2005) Large-scale synthesis of TiO_2 nanorods via nonhydrolytic sol-gel ester elimination reaction and their application to photocatalytic inactivation of E. coli. *J Phys Chem B* 109(32):15297–15302.
20. Mehdipour N, Mousavian N, Eslami H (2014) Molecular dynamics simulation of the diffusion of nanoconfined fluids. *J Iran Chem Soc* 11(1):47–52.
21. Eslami H, Jaafari B, Mehdipour N (2013) Coarse grained molecular dynamics simulation of nanoconfined water. *ChemPhysChem* 14(5):1063–1070.
22. Anderson K, et al. (2010) Microfluidic-based measurements of cytochrome P450 enzyme activity of primary mammalian hepatocytes. *Analyst (Lond)* 135(6):1282–1287.
23. Zhu Z, et al. (2013) Structure and chemical state of the Pt(557) surface during hydrogen oxidation reaction studied by in situ scanning tunneling microscopy and X-ray photoelectron spectroscopy. *J Am Chem Soc* 135(34):12560–12563.
24. Michalak WD, et al. (2014) CO oxidation on PtSn nanoparticle catalysts occurs at the interface of Pt and Sn oxide domains formed under reaction conditions. *J Catal* 312: 17–25.
25. Jaramillo TF, et al. (2007) Identification of active edge sites for electrochemical H2 evolution from MoS2 nanocatalysts. *Science* 317(5834):100–102.
26. Gulati A, Liao H, Hafner JH (2006) Monitoring gold nanorod synthesis by localized surface plasmon resonance. *J Phys Chem B* 110(45):22323–22327.
27. Martin JJ, Armington AF (1983) Effect of growth rate on quartz defects. *J Cryst Growth* 62(1):203–206.
28. Tachikawa T, Yamashita S, Majima T (2010) Probing photocatalytic active sites on a single titanosilicate zeolite with a redox-responsive fluorescent dye. *Angew Chem Int Ed Engl* 49(2):432–435.
29. Courty A, Henry A-I, Goubet N, Pileni M-P (2007) Large triangular single crystals formed by mild annealing of self-organized silver nanocrystals. *Nat Mater* 6(11): 900–907.
30. Millstone JE, et al. (2005) Observation of a quadrupole plasmon mode for a colloidal solution of gold nanoprisms. *J Am Chem Soc* 127(15):5312–5313.
31. DuChene J, et al. (2013) Halide anions as shape-directing agents for obtaining high-quality anisortropic gold nanostructures. *Chem Mater* 25(8):1392–1399.
32. Kim F, Connor S, Song H, Kuykendall T, Yang P (2004) Platonic gold nanocrystals. *Angew Chem Int Ed Engl* 43(28):3673–3677.
33. Muralidharan K, Simmons JH, Deymier PA, Runge K (2005) Molecular dynamics studies of brittle fracture in vitreous silica: Review and recent progress. *J Non-Cryst Solids* 351(18):1532–1542.
34. Buurmans IL, Weckhuysen BM (2012) Heterogeneities of individual catalyst particles in space and time as monitored by spectroscopy. *Nat Chem* 4(11):873–886.
35. Cordes T, Blum SA (2013) Opportunities and challenges in single-molecule and single-particle fluorescence microscopy for mechanistic studies of chemical reactions. *Nat Chem* 5(12):993–999.